Molecular dynamics simulations of the delta and omicron SARS-CoV-2 spike – ACE2 complexes reveal distinct changes between both variants

Eileen Socher [a,b,*], Lukas Heger [c], Friedrich Paulsen [a], Friederike Zunke [d], Philipp Arnold [a,*]

[a] Institute of Anatomy, Functional and Clinical Anatomy, Friedrich-Alexander Universität Erlangen-Nürnberg (FAU), Erlangen, Germany
[b] Institute for Clinical and Molecular Virology, Friedrich-Alexander Universität Erlangen-Nürnberg (FAU), University Hospital Erlangen, Erlangen, Germany
[c] Laboratory of Dendritic Cell Biology, Department of Dermatology, Friedrich-Alexander Universität Erlangen-Nürnberg (FAU), University Hospital Erlangen, Erlangen, Germany
[d] Department of Molecular Neurology, University Hospital Erlangen, Friedrich-Alexander Universität Erlangen-Nürnberg (FAU), Erlangen, Germany

ARTICLE INFO

ABSTRACT

SARS-CoV-2, the virus causing the COVID-19 pandemic, changes frequently through the appearance of mutations constantly leading to new variants. However, only few variants evolve as dominating and will be considered as "Variants of Concern" (VOCs) by the world health organization (WHO). At the end of 2020 the alpha (B.1.1.7) variant appeared in the United Kingdom and dominated the pandemic situation until mid of 2021 when it was substituted by the delta variant (B.1.617.2) that first appeared in India as predominant. At the end of 2021, SARS-CoV-2 omicron (B.1.1.529) evolved as the dominating variant. Here, we use *in silico* modeling and molecular dynamics (MD) simulations of the receptor-binding domain of the viral spike protein and the host cell surface receptor ACE2 to analyze and compare the interaction pattern between the wild type, delta and omicron variants. We identified residue 493 in delta (glutamine) and omicron (arginine) with altered binding properties towards ACE2.

1. Introduction

The COVID-19 pandemic caused by the novel severe acute respiratory syndrome coronavirus 2 (SARS-CoV-2) is driven by newly emerging variants that arise from the original virus. Although most of the genetic changes have little to no impact on the virus' properties, some virus variants arise with higher transmissibility and/or increased virulence. These variants are classified as "*Variants of Concern*" (VOC) by the WHO. In January 2022, the WHO listed five VOCs labeled with Greek letters [1]: (1) the alpha variant (Pango lineage: B.1.1.7) that emerged in the United Kingdom, (2) the beta variant (Pango lineage: B.1.351) from South Africa, (3) the gamma variant (Pango lineage: P.1) from Brazil, (4) the delta variant (Pango lineage: B.1.617.2) first detected in India and the omicron variant (Pango lineage: B.1.1.529) first identified in South Africa in November 2021 [2].

All these VOCs listed by the WHO acquired some distinctive mutations (Fig. 1a lists the mutations of the predominant delta and omicron variants) in the trimeric spike glycoprotein of SARS-CoV-2, which specifically binds with its receptor-binding domain (RBD) to the host cell receptor angiotensin-converting enzyme 2 (ACE2) [3–5]. This binding step is crucial for viral entry into a host cell to initiate infection (Fig. 1b) [6–7]. Therefore, understanding the interaction of the virus with ACE2 at the cell surface is fundamentally important in the fight against SARS-CoV-2. The protein structure of the RBD of the wild type spike protein in complex with ACE2 is known (e.g. PDB ID code: 7KMB [8]) and allows

* Corresponding authors at: Institute of Anatomy, Functional and Clinical Anatomy, Friedrich-Alexander Universität Erlangen-Nürnberg (FAU), Erlangen, Germany.
E-mail addresses: eileen.socher@fau.de (E. Socher), lukas.heger@uk-erlangen.de (L. Heger), friedrich.paulsen@fau.de (F. Paulsen), friederike.zunke@fau.de (F. Zunke), philipp.arnold@fau.de (P. Arnold).
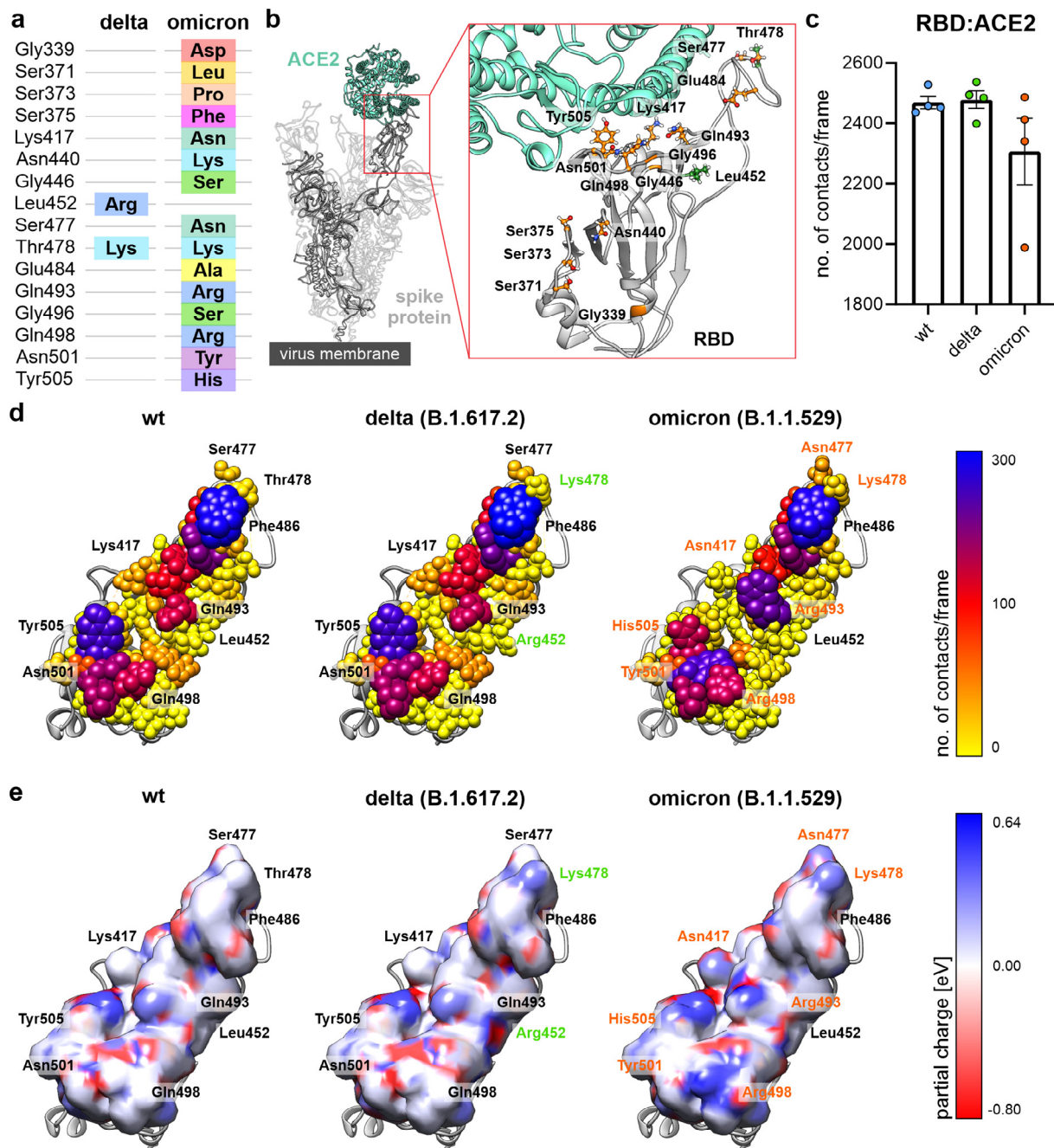
Fig. 1. Number of contacts and electrostatic potential. a, Amino acid exchanges at distinct positions in the delta and omicron variants. b, Structural representation of the SARS-CoV-2 spike protein on the viral membrane with the inset showing all residues mutated in delta (B.1.617.2, green) or omicron (B.1.1.529, orange). c, Number of contacts between the RBD and ACE2 for wt, delta and omicron (difference not significant). d, Structural representation of the interface of the RBD with ACE2 according to the number of contacts in color code. Residues with a green label are mutated in the delta variant and residues with an orange label are mutated in omicron. e, Surface representation of the interface formed by the RBD with ACE2. Surface coloring according to the electrostatic potential of the underlying residues with 0.64 eV in blue and −0.80 eV in red. (For interpretation of the references to color in this figure legend, the reader is referred to the web version of this article.)

characterization of receptor binding at the atomic level, greatly improving our understanding of host-pathogen interactions at this site. By introducing the observed mutations into the wild type RBD–ACE2 complex structure with *in silico* modeling and subsequently conducting molecular dynamics (MD) simulations of these RBD–ACE2 complexes, the influence of specific mutations in the RBD on binding towards the human receptor can be strongly enhanced [9–11]. Experimentally determined protein structures provide the basis for MD simulations, which can add information on the protein dynamics, the flexibility and residue interactions that would be difficult to access with experimental methods. Addi-

tionally, MD simulations can today often be performed and analyzed much faster than experimentally determined structures can be obtained and therefore it can serve as a predictive tool.

The mentioned alpha, beta, gamma and omicron variants harbor as common feature all a substitution of asparagine-to-tyrosine at position 501 (N501Y) in the RBD, which is not present in the delta variant [12]. In addition to the N501Y mutation, omicron carries 14 other mutations within the RBD (Fig. 1a). A considerable number of them can be found at the direct binding interface with ACE2 (Fig. 1b). In contrast to omicron, the delta variant has a characteristic leucine-to-arginine substitution at position 452

(L452R), which was detected earlier in the related kappa variant (B.1.617.1) and in an unrelated lineage in the United States of America (epsilon variant: B.1.427/B.1.429). For variants carrying this L452R mutation, stronger affinity of the spike protein for the ACE2 receptor was described [13–14]. The delta and omicron variants share a common T478K mutation and for delta reduced affinity of neutralizing antibodies at this position was shown [15–17]. In omicron many of the mutations found at the RBD are located within epitopes recognized by neutralizing antibodies. An exemplary array of such neutralizing antibodies [44,45] is shown in Supplementary Fig. 1 and experimental data suggests reduced binding of antibodies from patient sera [18–19]. Of note, especially antibodies binding at the RBD at the site of contact formation with ACE2 show high neutralization properties [20].

The present study compares the original wild type (wt), the delta variant and the similar variants epsilon and kappa with the omicron variant. We identify residue 493 within the RBD as a major difference between all three variants. In wt and delta residue 493 is a glutamine (Gln493) and we show that the delta variant amino acid exchange L452R induces a rearrangement in all three L452R carrying variants (epsilon, delta and kappa) that increases the number of contacts and the number of hydrogen bonds with ACE2 for Gln493. The omicron variant expresses an arginine at position 493 and this arginine forms very stable salt bridges with residues glutamate 35 (Glu35) and aspartate 38 (Asp38) of the host cell receptor ACE2. In previous reports [21] an exchange from glutamine to lysine was reported at position 493 and we can show, that the omicron variants with Q493R or Q493K show very similar changes in contact formation with ACE2. However, for Q493R we also identified salt bridge formation with aspartate 30 (Asp30) that was not observed for the Q493K mutation. Additionally, omicron also carries an amino acid exchange from lysine 417 to asparagine (K417N). The same mutation was already observed in the beta variant, while in the gamma variant lysine 417 is mutated to a threonine (K417T). In wild type, lysine 417 forms a very stable salt bridge with aspartate 30 from the ACE2 receptor and we could show that exchange to asparagine or threonine largely disrupts binding at this position [9].

Here, we show that major changes in interaction with ACE2 occur at positions 417, 493, 501 and at position 505 where a tyrosine is mutated to a histidine (Y505H). We also show, that many of the remaining amino acid exchanges occurring within the RBD do not largely influence binding to ACE2, but rather change epitope areas for neutralizing antibodies (e.g. N440K, G446S, T478K, E484A and G496S) [20], which might explain the reduced neutralization capacity identified for serum samples from vaccinated patients [18].

2. Results

2.1. The contact analyses and electrostatic potential of the viral receptor-binding domain

The SARS-CoV-2 delta and omicron variants have both acquired a threonine-to-lysine (T478K) substitution in the RBD. The delta variant carries an additional leucine-to-arginine (L452R) substitution in the RBD and the omicron variant has, in addition to this T478K mutation, 14 other mutations within the RBD (Fig. 1a). In order to compare individual virus variants, we performed four independent MD simulation runs over 500 ns for every variant's RBD in complex with ACE2. Subsequently, we analyzed the overall intermolecular contacts formed between the human ACE2 and the viral RBD of the wild type and the delta and omicron variants. We found a reduced number of contacts between the RBD and ACE2 for the omicron variant, while the number of contacts for the delta

variant was not markedly changed (Fig. 1c). Then, we assigned the individual number of contacts to all RBD amino acids within 8 Å distance to ACE2 and found marked differences for residues 493, 501 and 505 (Fig. 1d, Supplementary Fig. 2a). Wild type and delta variant express an asparagine at position 501, whereas the omicron variant harbors a tyrosine (N501Y) at this position. The functional consequences of this N501Y mutation were already described [22] and a cryo-electron microscopy structure carrying this N501Y exchange in complex with ACE2 was also experimentally solved (PDB ID code: 7MJN [23]). In the omicron variant, the tyrosine at position 505 (wt and delta variant) is mutated to histidine and we identified a reduced number of contacts to ACE2 for histidine at this position (Fig. 1d, Supplementary Fig. 2a and Supplementary Fig. 2b). In detail, residue 505 interacts with the carbon atoms of the side chain of lysine 353 on ACE2 (Supplementary Fig. 2c). Here a pi-electron ring system (as for tyrosine expressing variants) might have more contacts than the inserted histidine in omicron. For the epsilon (B.1.427/B.1.429) and kappa (B.1.617.1) variant, we also performed contact analyses and found no marked differences on the individual amino acid level (Supplementary Fig. 2d). As the omicron variant shows a considerable number of positively charged amino acids at sites of mutation, we analyzed the electrostatic potential at the RBD-ACE2 interface and found increased electro positivity in the delta variant (L452R and T478K) and even more pronounced in the omicron variant (T478K, Q493R, Q498R and Y505H; Fig. 1e). However, the omicron variant also loses a positively charged amino acid at the interaction interface at position 417 (K417N; Fig. 1b, Fig. 1e).

2.2. The interaction between residue 493 and ACE2 is altered in delta and omicron variant

As numerous positively charged amino acids appear at the interaction interface, we also analyzed the linear electrostatic interaction energy to identify newly formed or resolved intermolecular salt bridges. Largest differences between wt, delta and omicron were found at positions 417 and 493 (Fig. 2a, Supplementary Fig. 3). Analyzing the electrostatic potential at the interaction interface on ACE2 revealed aspartate 30, glutamate 35 and aspartate 38 as potential interaction partners for these two residues (Fig. 2b). For other variants that exchanged lysine 417 to asparagine or threonine, we already identified a strongly reduced electrostatic interaction energy with aspartate 30 [9]. Thus it was not very surprising that we found the same reduction for the omicron variant (Fig. 2c) and a salt bridge in wt (Fig. 2d) that also remains stable over time (Fig. 2e, Table S1). Next, we analyzed contact formation for residue 493 (Fig. 2f). We found that wt and delta (both with Gln493) behave similar, but that omicron shows some major differences. The delta variant shows a small increase in contact formation with lysine 31 and glutamate 35 (Fig. 2f). In contrast, omicron changes its interaction profile completely. For one MD simulation run we identified interaction with aspartate 30 (Asp30) and in three runs increased interaction with glutamate 35 (Glu35) and with aspartate 38 (Asp38). Additionally, the interaction with lysine 31 (Lys31) is reduced in all four simulation runs of the omicron variant (Fig. 2f) probably due to electrostatic repulsion between the positively charged arginine 493 and the also positively charged lysine 31.

2.3. The delta variant shows increased hydrogen bond formation with ACE2

To analyze changes in the delta variant, we pooled it with four individual MD simulation runs of the epsilon and four runs of the kappa variant (all these variants carry the L452R mutation) and compared it to twelve 500 ns long simulation runs of the wt
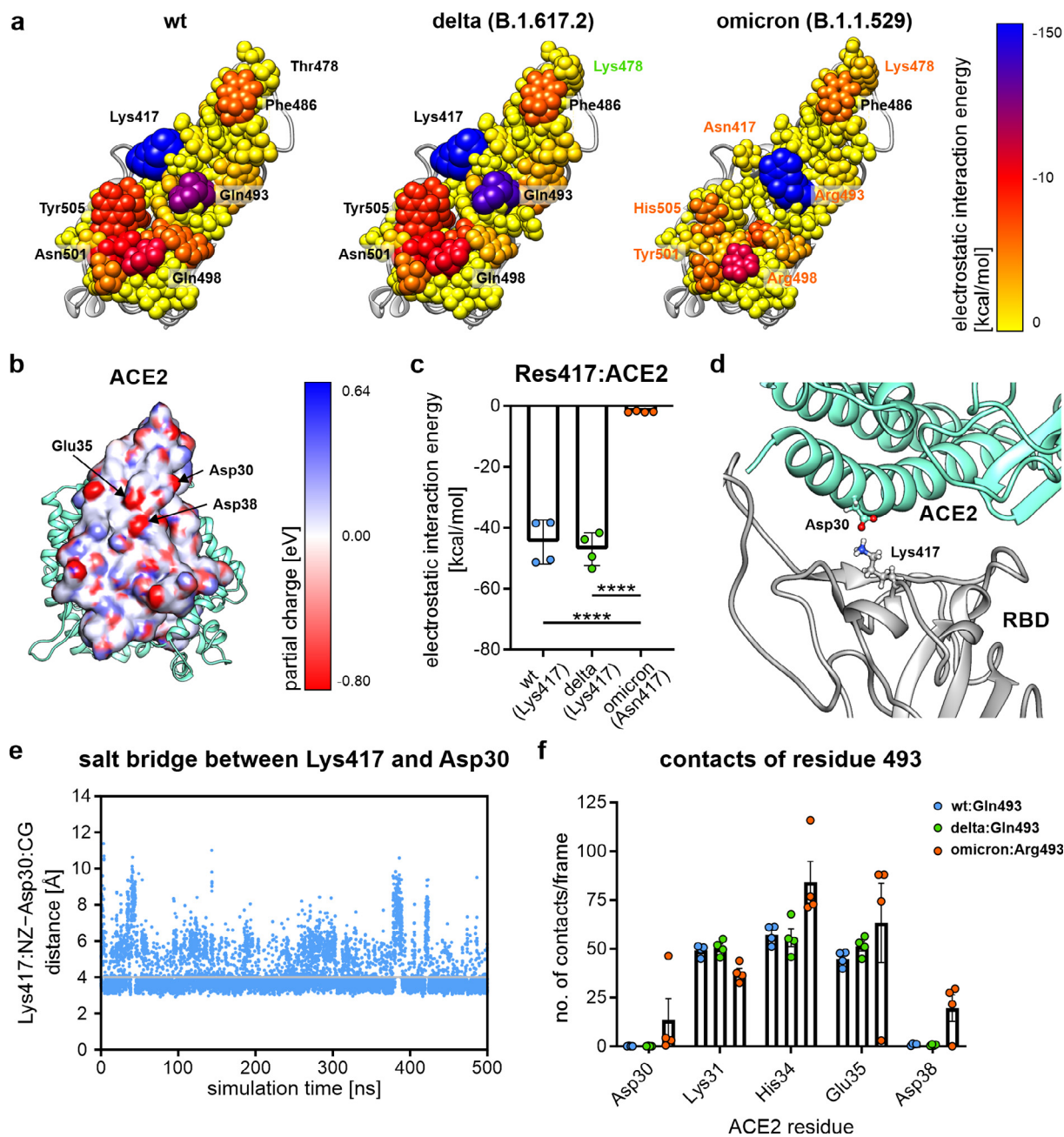
Fig. 2. Linear electrostatic interaction shows two major changes in omicron. a, Structural representation of the RBD interface with ACE2 with residues shown as spheres with their size and color according to their electrostatic interaction. b, Surface representation of the binding interface of ACE2 with the RBD. Surface color is labeled according to the partial charge of the underlying residues with the three negatively charged residues aspartate 30 (Asp30), glutamate 35 (Glu35) and aspartate 38 (Asp38). c, Linear electrostatic binding energy of residue 417 in wt (blue), delta (green) and omicron (orange; **** p < 0.0001 one-way ANOVA). d, Structural representation of the salt bridge formed by lysine 417 (Lys417) from the RBD and aspartate 30 (Asp30) from ACE2 in the wt complex. e, Time resolved distance plot of the distance between side chain atoms of Lys417 and Asp30 in the wt complex. f, Number of contacts per frame formed by residue 493 with interacting ACE2 residues (differences are not significantly different). (For interpretation of the references to color in this figure legend, the reader is referred to the web version of this article.)

RBD–ACE2 complex (eight of them were already described earlier [9,10]). Within the neighboring beta sheet of glutamine 493, the L452R exchange can be found (Fig. 3a, b), thereby changing the structural environment of glutamine 493. We found that the number of intermolecular contacts between glutamine 493 and the human receptor ACE2 increases in the different L452R variants compared to wild type RBD–ACE2 complexes (Fig. 3c). Decomposed on the individual amino acid level, although not significant, we identified the ACE2 residues glutamate 35 and to a minor extend lysine 31 with an increased number of contacts to glutamine 493 (Fig. 3d,e). Contact formation between glutamine 493

and histidine 34 of ACE2 was unchanged, however (Fig. 3d,e). As glutamine residues engage in hydrogen bonds, we also analyzed the number of intermolecular hydrogen bonds of glutamine 493 with ACE2 and found a significant increase for variants that express the L452R mutation (Fig. 3f). Detailed analysis showed an increased occurrence of hydrogen bonds with lysine 31 and with glutamate 35 (Fig. 3g, Tables S2, S3). The structural representation illustrates that the side chain oxygen atom of glutamine 493 forms a hydrogen bond with the side chain of lysine 31 from ACE2 while one of the hydrogens of the amino group forms hydrogen bonds with the oxygen atoms of the carboxyl group of glutamate
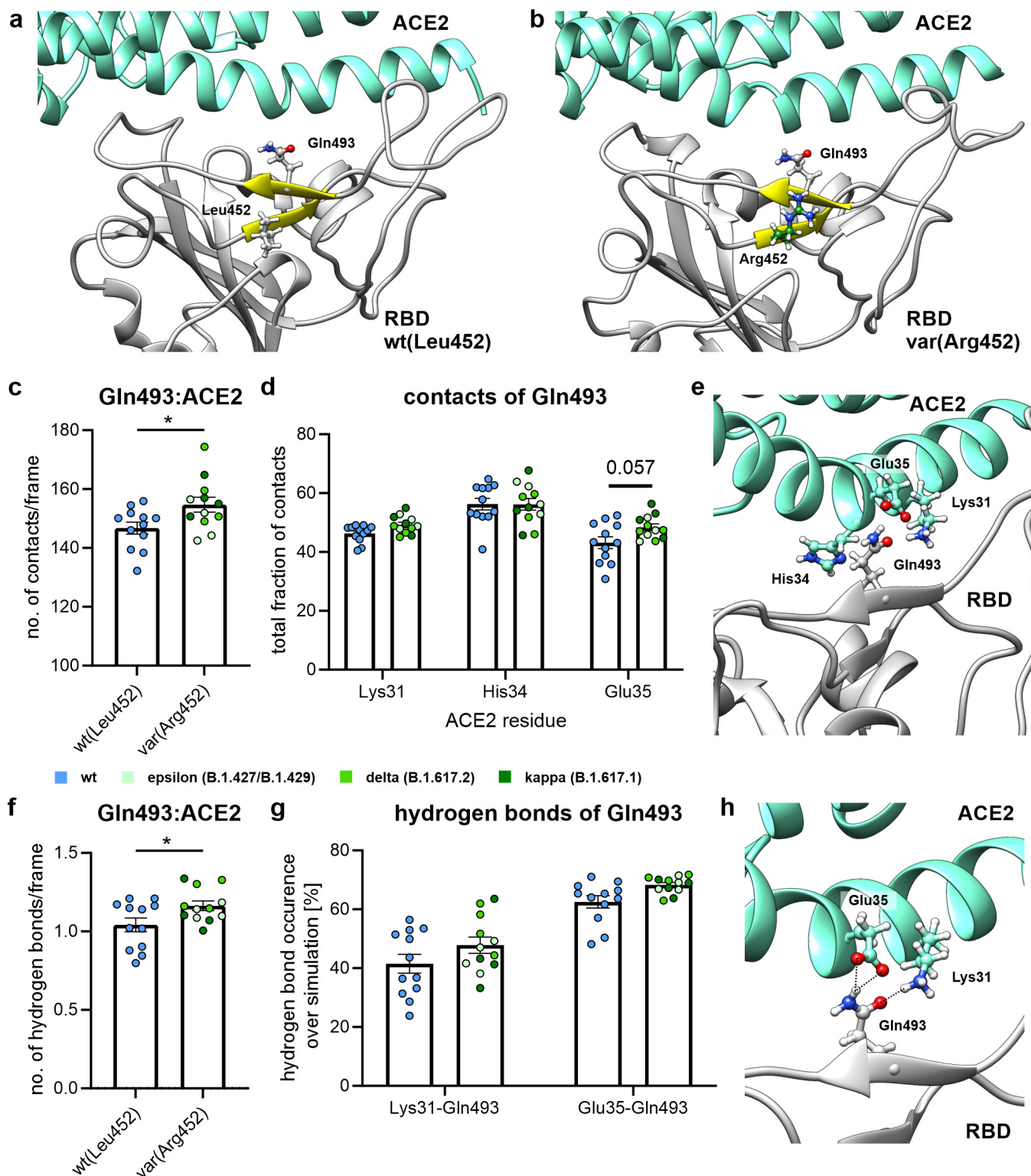
Fig. 3. Hydrogen bond rearrangement in delta. a, Structural representation of the glutamine 493 (Gln493) and leucine 452 (Leu452) as expressed on two neighboring β-strands forming a small 2-stranded antiparallel β-sheet (yellow) in wt. b, As in figure panel a, but with residue 452 exchanged to arginine (Arg452, green) as expressed on delta (medium green), epsilon (light green) and kappa (dark green) variants. c, Combined analysis of wt and three variants that carry the leucine 452 arginine (L452R) exchange with regard to the number of contacts formed by glutamine 493 (Gln493) with ACE2 (* p < 0.05, two-tailed Student's T-test). d, Residue specific analysis of the number of contacts between wt and L452R expressing variants (one-way ANOVA). e, Structural representation of glutamine 493 (Gln493) expressed on the RBD and its interaction partners from ACE2 lysine 31 (Lys31), histidine 34 (His34) and glutamate 35 (Glu35). f, Number of hydrogen bonds formed by glutamine 493 (Gln493) per frame comparing wt and L452R expressing variants (* p < 0.05, two-tailed Student's T-test).g, Hydrogen bond formation between glutamine 493 (Gln493) from the RBD and lysine 31 (Lys31) and glutamate 35 (Glu35, both ACE2). h, Structural representation of the hydrogen bonds formed between glutamine 493 (Gln493, RBD) and lysine 31 (Lys31, ACE2) and glutamate 35 (Glu35, ACE2). (For interpretation of the references to color in this figure legend, the reader is referred to the web version of this article.)

35 (Fig. 3h). A detailed root-mean-square fluctuation (RMSF) analysis (Supplementary Fig. 4a) showed a reduced flexibility for the entire glutamine 493 (Supplementary Fig. 4b) and especially for side chain atoms of the amino group (NE2, HE21 and HE22; Supplementary Fig. 4b) in the different L452R variants compared to wild type RBD–ACE2 complexes. This reduced flexibility of glutamine's side chain atoms can be observed due to the stronger hydrogen bond network of glutamine 493 with ACE2, which stabilizes the side chain position. Histidine 34 does not form hydrogen bonds with glutamine 493, but forms a hydrogen bond with tyrosine 453 (Supplementary Fig. 4c,d). Together, we can conclude that the delta variant shows an increase in contacts and consequently in hydrogen bond formation of glutamine 493 with ACE2 and that this might contribute to an increased binding.

2.4. The omicron variant forms two new stable salt bridges with ACE2 residues

As described above (Fig. 2f), we identified an entirely altered interaction pattern for arginine at position 493. The number of contacts with glutamate 35 increased and contacts with aspartate 38 were newly formed and not present in variants expressing a glutamine at position 493 (Fig. 2f). For three of our MD simulations, these two newly formed salt bridges can also be appreciated in time course distance plots of arginine 493 with aspartate 30, glutamate 35 and aspartate 38 (Fig. 4a; Supplementary Fig. 5a). However, one of our MD simulation runs showed a different picture and we found a stable intermolecular salt bridge between arginine 493 and aspartate 30 on ACE2 (Fig. 4b). Analyzing the average distances to favored residues on ACE2 within single runs provided insight into the stability of the individual salt bridges (Fig. 4c). Especially interactions between arginine 493 and aspartate 30 and glutamate 35 show low standard deviations with average distances below 5 Å, thus strongly supporting ionic interaction. Analysis of the linear electrostatic interaction energy at position 493 showed a strong increase for omicron when compared to wt and delta (Fig. 4d). Thus, we can now postulate two different interactions with ACE2 for arginine at position 493 in the omicron variant. In the first mode, it forms salt bridges and hydrogen bonds with glutamate 35 and aspartate 38 (Fig. 4e, Table S4) and in the second mode it forms a salt bridge and hydrogen bonds with aspartate 30 (Fig. 4f, Table S4). Within the same simulation run, where we identified a stable salt bridge between arginine 493 and aspartate 30 from ACE2, we also identified a stable salt bridge between arginine 498 (only present in omicron) and aspartate 38 (Fig. 4f, Supplementary Fig. 5b). Together, omicron carrying an arginine at position 493 (Q493R) shows a higher flexibility in contact formation than wt or delta in the same region. As there was a sequence conflict at position 493 at the beginning, we also simulated the RBD-ACE2 complex with a lysine at this position 493. All runs showed stable salt bridges between lysine 493 and glutamate 35 (Supplementary Fig. 6a,b) and aspartate 38 (Supplementary Fig. 6c,d) of ACE2. A lysine side chain at this position might be too short to interact with aspartate 30 (Supplementary Fig. 6e). The increase in linear electrostatic interaction energy, however, remains similar (Supplementary Fig. 6f). One selection advantage of the omicron over the omicron + Q493K variant might be the more flexible interaction regime at this position.

3. Discussion

The appearance of a L452R exchange within the RBD of the SARS-CoV-2 spike protein rendered the affected variants to former "Variants under Investigation" (epsilon, kappa) or current "Variant of Concern" (delta variant) [1]. The delta variant dominated the

pandemic worldwide from mid-2021. All three variants carry additional amino acid exchanges within the other parts of the spike protein, including the D614G variant that we identified as a potential molecular switch to liberate the fusion peptide [10]. Here, we show that the L452R mutation induces an increased number of hydrogen bonds formed by glutamine 493 between the RDB (delta variant) and ACE2. Glutamine 493 was also identified as an important interaction residue in the original wt SARS-CoV-2 virus [24–26]. The increased number of hydrogen bonds in delta might induce a stronger interaction between RBD and ACE2 and thus support increased viral infectivity. Comparing the omicron variant to wt and delta reveals major differences in RBD-ACE2 interaction. As in the alpha variant, omicron carries a N501Y mutation and, as the beta variant, carries the K417N mutation. Both residues are important for RBD–ACE2 interaction in wt [24,26] and the N501Y mutation apparently increases the binding energy between RBD and ACE2 and the K417N mutation reduces it [22]. Before delta dominated the pandemic starting mid-2021, the alpha variant outcompeted the wt SARS-CoV-2 variant end of 2020/beginning of 2021. Parallel with the alpha variant, the beta and gamma variants appeared both with exchanges for lysine at position 417 that induced a loss of the salt bridge at this position [9,24]. In omicron this salt bridge is also lost. However, through the exchange of glutamine 493 to an arginine (Q493R), two additional salt bridges are formed (either by arginine 493 itself or by arginine 498) and a strong increase in linear electrostatic interaction energy can be observed. The variability in salt bridge formation at positions 493 and 498 might increase the probability for RBD-ACE2 interaction and thereby increase infectivity. The original glutamine at position 498 is engaged in hydrogen bond formation with ACE2, thus residue 498 is consistently involved in RBD–ACE2 interaction [9,24–26]. As a side note, we could also show that a lysine at this position has a less flexible interaction pattern. Overall, three mutations within the RBD of omicron can be attributed to direct changes in interaction with ACE2 and these are K417N, Q493R and N501Y. With the exchange of tyrosine 505 to histidine, a reduced number of contacts is associated. However, the effect of this exchange cannot be fully judged. When comparing the delta and omicron variant to wt an additional trend becomes evident. Amino acid exchanges within the RBD render it more electropositive. Delta is more positive than wt and omicron more positive than delta. This might enable a better passive adhesion to the negatively charged glycocalyx and here especially to heparin sulfate, which is a critical factor for SARS-CoV-2 binding [27–29]. Thus, we can identify amino acid exchanges which (i) influence direct interaction with ACE2, (ii) change epitopes of neutralizing antibodies and/or (iii) change the electrostatic surface potential. In omicron, five of the fifteen mutations within the RBD insert positively charged amino acids (N440K, T478K, Q493R, Q498R and Y505H) and only one is lost (K417N). All of these six positions are within epitope regions for neutralizing antibodies [20]. In conclusion, omicron started to dominate the pandemic at the end of 2021 with patient numbers rising steeply in affected areas. MD simulation and structural analysis of the RBD-ACE2 complex shows clear differences of the omicron to the delta variant. Omicron has progressed in terms of ACE2 binding, in terms of immune escape and presents a more positively charged interface area.

4. Methods

4.1. Generation of the starting structures

To investigate the interface between the RBD of the spike protein and ACE2, the respective wild type start structure was taken from the PDB database (PDB ID code: 7KMB [8]). To also generate
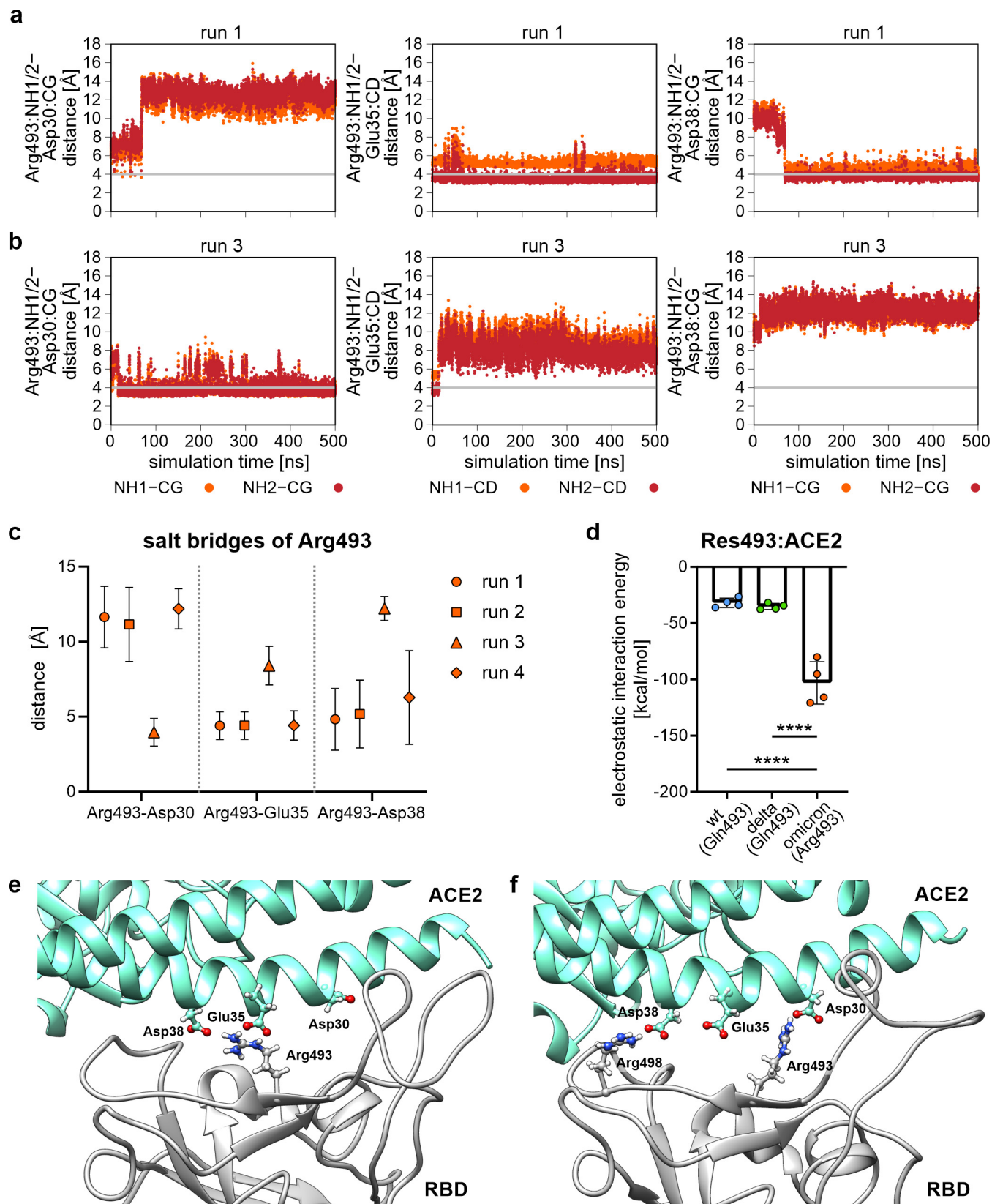
Fig. 4. Newly formed salt bridges in omicron between arginine 493 and negatively charged residues on ACE2. a, Representative distance plots of arginine 493 (RBD, omicron) and aspartate 30 (Asp30), glutamate 35 (Glu35) and aspartate 38 (Asp38) (all three on ACE2). b, Distance plots of a different MD simulation run than shown in figure panel a between the same residues. c, Average distance with standard deviation error bars shown for four individual 500 ns runs for residues arginine 493 (RBD, omicron) and aspartate 30 (Asp30), glutamate 35 (Glu35) and aspartate 38 (Asp38). d, Linear electrostatic interaction energy for residue 493 analyzed for wt (blue), delta (green) and omicron (orange; **** $p < 0.0001$, one-way ANOVA). e, Structural representation of the two newly formed salt bridges between arginine 493 (Arg493) on the RBD and glutamate 35 (Glu35) and aspartate 38 (Asp38) both expressed on ACE2. f, Structural representation of salt bridges formed between Arg493 (RBD) and Asp30 (ACE) and Arg498 (RBD) and Asp38 (ACE2). (For interpretation of the references to color in this figure legend, the reader is referred to the web version of this article.)

the starting structures for the MD simulations of the different SARS-CoV-2 variants, the amino acid substitutions (epsilon spike variant (B.1.427/B.1.429): L452R; delta variant (B.1.617.2): L452R and T478K; kappa variant (B.1.617.1): L452R and E484Q, omicron variant (B.1.1.529): G339D, S371L, S373P, S375F, K417N, N440K, G446S, S477N, T478K, E484A, Q493R, G496S, Q498R, N501Y, Y505H and for an omicron variant with a lysine at position 493: G339D, S371L, S373P, S375F, K417N, N440K, G446S, S477N, T478K, E484A, Q493K, G496S, Q498R, N501Y, Y505H) were introduced with Swiss-PdbViewer 4.1.0 [30] (http://www.expasy.org/spdbv/).

For the electrostatic analyses of the protein surface, "PQR" output files were generated by using charge parameters assigned with the APBS-PDB2PQR software suite [31] (https://server.poisson-boltzmann.org/).

4.2. Molecular dynamics simulations

Molecular dynamics simulations were performed exactly as described before [9–10]. By using version 20 of the Amber Molecular Dynamics software package (ambermd.org) [32], the ff14SB force field [33] and the Amber Tool LEaP, all systems were electrically neutralized with Na^+ ions and solvated with TIP3P [34] water molecules. The receptor-binding domain complexed with ACE2 was solvated in a water box with the shape of a truncated octahedron and a distance of at least 25 Å from the borders to the solute.

Minimization was carried out in three consecutive parts to optimize the geometry of the initial structures. In the first minimization part, all water molecules were minimized, while all other atoms were restrained at the initial positions by using a constant force of 10 kcal·mol^{-1}·Å^{-2}. During the second part, additional relaxation of the sodium ions and the hydrogen atoms of the protein was allowed, while the remaining protein was restrained with 10 kcal·mol^{-1}·Å^{-2}. In the third part, the entire protein, ions, and water molecules were minimized without any restraints. All three minimization parts started with 2500 steps using the steepest descent algorithm, followed by 2500 steps of a conjugate gradient minimization. After minimization, the systems were equilibrated in two successive steps. In the first step, the temperature was increased from 10 to 310 K within 0.1 ns and the protein was restrained with a constant force of 5 kcal·mol^{-1}·Å^{-2}. In the second step (0.4 ns length), only the C_α atoms of the protein were restrained with a constant force of 5 kcal·mol^{-1}·Å^{-2}. In both equilibration steps, the time step was 2 fs. Minimization and equilibration were carried out on CPUs, while the subsequent production runs were performed using pmemd.CUDA on Nvidia A100 GPUs [35–37]. Subsequent 500 ns long production runs were performed without any restraints and at 310 K (regulated by a Berendsen thermostat [38]). Furthermore, the constant pressure periodic boundary conditions with an average pressure of 1 bar and isotropic position scaling were used. For bonds involving hydrogen, the SHAKE algorithm [39] was applied in the equilibration and production phases. To accelerate the production phase of the MD simulations, hydrogen mass repartitioning (HMR) [40] was used in combination with a time step of 4 fs. For statistical analyses, four independent 500 ns long MD simulation runs were performed for the epsilon, delta, kappa and omicron spike protein RBD variants in complex with ACE2. For the wild type RBD in complex with ACE2 16 independent 500 ns long MD simulation runs were used (eight completely new MD simulations and in addition also eight MD simulation runs conducted for two earlier studies [9–10] were re-evaluated).

Trajectory analysis (analysis of root-mean-square fluctuations (RMSF), analysis of contacts (always with distance criterion of ≤ 5 Å between any pair of atoms; total fraction of contacts for residue pairs), measurement of interatomic distances, calculation of electrostatic linear interaction energy and hydrogen bond analyses were performed using the Amber tool cpptraj [41]. Per-residue free energy decomposition for calculation of the energy contribution of single residues was performed with MMPBSA.py [42].

4.3. Statistics and display

Statistical analyses were performed with GraphPad Prism (version 9.2.0 for Windows, GraphPad Software, San Diego, California USA, www.graphpad.com) and statistical tests were applied as indicated below the figure. Plots were created in GraphPad and all structure images were made with UCSF Chimera 1.15 [43].

CRediT authorship contribution statement

Eileen Socher: Conceptualization, Validation, Formal analysis, Investigation, Data curation, Writing – original draft, Writing – review & editing, Visualization. **Lukas Heger:** Validation, Writing – review & editing. **Friedrich Paulsen:** Resources, Writing – review & editing. **Friederike Zunke:** Validation, Writing – review & editing, Funding acquisition. **Philipp Arnold:** Conceptualization, Validation, Formal analysis, Data curation, Writing – original draft, Writing – review & editing, Visualization, Funding acquisition.

Declaration of Competing Interest

The authors declare that they have no known competing financial interests or personal relationships that could have appeared to influence the work reported in this paper.

Acknowledgments

Appendix A. Supplementary data

Supplementary data to this article can be found online at https://doi.org/10.1016/j.csbj.2022.02.015.

References

[1] WHO. https://www.who.int/en/activities/tracking-SARS-CoV-2-variants. (2022).

[2] Wang L, Cheng, G. Sequence analysis of the emerging SARS-CoV-2 variant Omicron in South Africa. *Journal of Medical Virology* **n/a**.

[3] Hoffmann M et al. SARS-CoV-2 cell entry depends on ACE2 and TMPRSS2 and is blocked by a clinically proven protease inhibitor. Cell 2020;181:271–280 e8.

[4] Yang J et al. Molecular interaction and inhibition of SARS-CoV-2 binding to the ACE2 receptor. Nat Commun 2020;11:4541.

[5] Li W et al. Angiotensin-converting enzyme 2 is a functional receptor for the SARS coronavirus. Nature 2003;426:450–4.

[6] Jackson CB, Farzan M, Chen B, Choe H. Mechanisms of SARS-CoV-2 entry into cells. Nat Rev Mol Cell Biol 2022;23:3–20.

[7] Zhou P et al. A pneumonia outbreak associated with a new coronavirus of probable bat origin. Nature 2020;579:270–3.

[8] Zhou T et al. Cryo-EM Structures of SARS-CoV-2 Spike without and with ACE2 Reveal a pH-dependent switch to mediate endosomal positioning of receptor-binding domains. Cell Host Microbe 2020;28:867–879 e5.

[9] Socher E et al. Computational decomposition reveals reshaping of the SARS-CoV-2-ACE2 interface among viral variants expressing the N501Y mutation. J Cell Biochem 2021;122:1863–72.

[10] Socher E et al. Mutations in the B.1.1.7 SARS-CoV-2 Spike Protein Reduce Receptor-Binding Affinity and Induce a Flexible Link to the Fusion Peptide. Biomedicines 2021;9.

[11] Jawad B, Adhikari P, Podgornik R, Ching WY. Key Interacting Residues between RBD of SARS-CoV-2 and ACE2 receptor: combination of molecular dynamics simulation and density functional calculation. J Chem Inf Model 2021;61:4425–41.

[12] ECDC. https://www.ecdc.europa.eu/en/covid-19/variants-concern. (2021).

[13] Khan MI et al. Impact of the Double Mutants on Spike Protein of SARS-CoV-2 B.1.617 Lineage on the Human ACE2 Receptor Binding: A Structural Insight. Viruses 2021;13.

[14] Deng X et al. Transmission, infectivity, and antibody neutralization of an emerging SARS-CoV-2 variant in California carrying a L452R spike protein mutation. medRxiv 2021.

[15] Wilhelm A et al. Antibody-Mediated Neutralization of Authentic SARS-CoV-2 B.1.617 Variants Harboring L452R and T478K/E484Q. Viruses 2021;13.

[16] Focosi D, Maggi F. Neutralising antibody escape of SARS-CoV-2 spike protein: Risk assessment for antibody-based Covid-19 therapeutics and vaccines. Rev Med Virol 2021;31:e2231.

[17] Liu C et al. Reduced neutralization of SARS-CoV-2 B.1.617 by vaccine and convalescent serum. Cell 2021;184:4220–4236.e13.

[18] Wilhelm A et al. Reduced Neutralization of SARS-CoV-2 Omicron Variant by Vaccine Sera and monoclonal antibodies. medRxiv 2021.

[19] Dejnirattisai W et al. Reduced neutralisation of SARS-CoV-2 omicron B.1.1.529 variant by post-immunisation serum. Lancet 2021.

[20] Dejnirattisai W et al. The antigenic anatomy of SARS-CoV-2 receptor binding domain. Cell 2021;184:2183–2200 e22.

[21] ECDC. Implications o f the emergence and spread of the SARS CoV 2 B.1.1. 529 variant of concern (Omicron) for the EU/EEA. (2021).

[22] Starr TN et al. Deep mutational scanning of SARS-CoV-2 receptor binding domain reveals constraints on folding and ACE2 binding. Cell 2020;182:1295–1310 e20.

[23] Zhu X et al. Cryo-electron microscopy structures of the N501Y SARS-CoV-2 spike protein in complex with ACE2 and 2 potent neutralizing antibodies. PLoS Biol 2021;19:e3001237.

[24] Wang Y, Liu M, Gao J. Enhanced receptor binding of SARS-CoV-2 through networks of hydrogen-bonding and hydrophobic interactions. Proc Natl Acad Sci U S A 2020;117:13967–74.

[25] de Andrade J, Goncalves PFB, Netz PA. Why does the novel coronavirus spike protein interact so strongly with the human ACE2? A Thermodynamic Answer. Chembiochem 2021;22:865–75.

[26] Marti D et al. Unravelling the molecular interactions between the SARS-CoV-2 RBD spike protein and various specific monoclonal antibodies. Biochimie 2022;193:90–102.

[27] Wadowski PP et al. Glycocalyx as Possible Limiting Factor in COVID-19. Front Immunol 2021;12:607306.

[28] Lang J et al. Inhibition of SARS pseudovirus cell entry by lactoferrin binding to heparan sulfate proteoglycans. PLoS ONE 2011;6:e23710.

[29] Clausen TM et al. SARS-CoV-2 Infection Depends on Cellular Heparan Sulfate and ACE2. Cell 2020;183:1043–1057 e15.

[30] Guex N, Peitsch MC. SWISS-MODEL and the Swiss-PdbViewer: an environment for comparative protein modeling. Electrophoresis 1997;18:2714–23.

[31] Jurrus E et al. Improvements to the APBS biomolecular solvation software suite. Protein Sci 2018;27:112–28.

[32] Case DA et al. AMBER 2020.

[33] Maier JA et al. ff14SB: Improving the Accuracy of Protein Side Chain and Backbone Parameters from ff99SB. J Chem Theory Comput 2015;11:3696–713.

[34] Jorgensen WL, Chandrasekhar J, Madura JD, Impey RW, Klein ML. Comparison of simple potential functions for simulating liquid water. J Chem Phys 1983;79:926–35.

[35] Götz AW et al. Routine microsecond molecular dynamics simulations with AMBER on GPUs. 1. Generalized Born. J Chem Theory Comput 2012;8:1542–55.

[36] Salomon-Ferrer R, Götz AW, Poole D, Le Grand S, Walker RC. Routine microsecond molecular dynamics simulations with AMBER on GPUs. 2. Explicit solvent particle mesh Ewald. J Chem Theory Comput 2013;9:3878–88.

[37] Le Grand S, Götz AW, Walker RC. SPFP: Speed without compromise—a mixed precision model for GPU accelerated molecular dynamics simulations. Comput Phys Commun 2013;184:374–80.

[38] Berendsen HJC, Postma JPM, Gunsteren WFv, DiNola A, Haak JR. Molecular dynamics with coupling to an external bath. J Chem Phys 1984;81:3684–90.

[39] Jean-Paul Ryckaert GC, Berendsen Herman JC. Numerical integration of the Cartesian equations of motion of a system with constraints: molecular dynamics of n-alkanes. J Comput Phys 1977;23:327–41.

[40] Hopkins CW, Le Grand S, Walker RC, Roitberg AE. Long-time-step molecular dynamics through hydrogen mass repartitioning. J Chem Theory Comput 2015;11:1864–74.

[41] Roe DR, Cheatham 3rd TE. PTRAJ and CPPTRAJ: software for processing and analysis of molecular dynamics trajectory data. J Chem Theory Comput 2013;9:3084–95.

[42] Miller 3rd BR et al. MMPBSA.py: an efficient program for end-state free energy calculations. J Chem Theory Comput 2012;8:3314–21.

[43] Pettersen EF et al. UCSF Chimera—a visualization system for exploratory research and analysis. J Comput Chem 2004;25:1605–12.

[44] Barnes CO et al. SARS-CoV-2 neutralizing antibody structures inform therapeutic strategies. Nature 2020;588:682–7.

[45] Hansen J et al. Studies in humanized mice and convalescent humans yield a SARS-CoV-2 antibody cocktail. Science 2020;369:1010–4.